Effect of Sustainable Aviation Fuels on Contrail Formation Across Flight Routes: A Thermodynamic Analysis

Effet des carburants aéronautiques durables sur la formation de traînées de condensation à travers les routes de vol: une analyse thermodynamique

Zoya Sharma[1*]

1. Liberal Arts & Science Academy, Austin, Texas, USA
*Corresponding author. Email: zoya.sharma@g.austincc.edu

Abstract | Résumé

Aviation-induced contrail cirrus is known to be responsible for significant climate impact, yet fuel and engine-based mitigation strategies receive less emphasis than flight path and altitude optimization research. Flight path optimization studies require an enormous amount of multiparty coordination, real-time data collection, and resource-rich research partners. This study assesses the impact of sustainable aviation fuels (SAFs) on contrail formation, which is a research avenue more amenable to modeling. The usage of three SAF types, Hydroprocessed Esters and Fatty Acids Synthetic Paraffinic Kerosene (HEFA-SPK), Fischer-Tropsch Synthetic Paraffinic Kerosene (FT-SPK), and Alcohol-to-Jet Synthetic Paraffinic Kerosene (ATJ-SPK), was modeled on four representative flight routes. A mathematical framework based on the Schmidt-Appleman criterion (SAC) was developed. This framework was applied to atmospheric data at each waypoint along great circle routes for the four flight paths, enabling spatially resolved contrail formation probabilities to be evaluated for each fuel type. All three SAFs produced a marginal increase in mean contrail formation probability relative to baseline kerosene across all routes. This result is attributed to the higher water vapor emission indices and specific combustion heat of SAFs, which increase the slope parameter G and shift the threshold temperatures toward warmer values. However, this thermodynamic effect operates independently of the primary mitigatory mechanism of SAFs: the reduction of non-volatile particulate matter (nvPM) emissions. The reduced nvPM emissions suppress ice crystal nucleation through a distinct physical pathway not captured within the thermodynamic framework. The results therefore represent a worst-case estimate of contrail formation probability, and the full climate benefit of SAF deployment is expected to be realized when nvPM effects are incorporated alongside the thermodynamic assessment presented here.

———

Le cirrus de traînée induit par l'aviation est reconnu pour être responsable d'un impact climatique important, pourtant les stratégies d'atténuation basées sur le carburant et le moteur reçoivent moins d'attention que la recherche sur l'optimisation de la trajectoire de vol et de l'altitude. Les études d'optimisation de trajectoire de vol nécessitent une énorme coordination multipartite, une collecte de données en temps réel et des partenaires de recherche riches en ressources. Cette étude évalue l'impact des carburants aéronautiques durables (SAF) sur la formation de traînées de condensation, qui constitue une voie de recherche plus propice à la modélisation. L'utilisation de trois types de SAF, esters hydrotraités et acides gras (kérosène paraffinique synthétique HEFA-SPK), kérosène paraffinique synthétique Fischer-Tropsch (FT-SPK) et kérosène paraffinique synthétique alcool-à-jet (ATJ-SPK), a été modélisée sur quatre routes de vol représentatives. Un cadre mathématique basé sur le critère de Schmidt-Appleman (SAC) a été développé. Ce cadre a été appliqué aux données atmosphériques à chaque point de passage le long de chacune des quatre trajectoires de vol orthodromiques, permettant d'évaluer spatialement les probabilités de formation de traînées de condensation pour chaque type de carburant. Les trois SAF ont produit une augmentation marginale de la probabilité moyenne de formation de traînées par rapport au kérosène de base sur toutes les voies. Ce résultat est attribué aux indices d'émission de vapeur d'eau plus élevés et à la chaleur de combustion spécifique des SAF, qui augmentent le paramètre de pente G et déplacent les températures seuils vers des valeurs plus chaudes. Cependant, cet effet thermodynamique fonctionne indépendamment du principal mécanisme d'atténuation des SAF : la réduction des émissions de particules non volatiles (nvPM). Les émissions réduites de nvPM suppriment la nucléation des cristaux de glace par une voie physique distincte non capturée dans le cadre thermodynamique. Les résultats représentent donc une estimation dans le pire des cas de la probabilité de formation de traînées de condensation, et on s'attend à ce que le bénéfice climatique complet du déploiement du SAF soit réalisé lorsque les effets nvPM sont intégrés à l'évaluation thermodynamique présentée ici.

Keywords: Sustainable aviation fuels (SAFs), contrail formation, Schmidt-Appleman criterion, aviation climate impact, contrail cirrus, non-volatile particulate matter (nvPM), radiative forcing, flight route modelling.

Introduction

While carbon dioxide (CO_2) emissions from aircrafts create long-term effects, non-CO_2 components such as water vapor, nitrogen oxides (NOx), and soot also contribute significantly to atmospheric warming through the formation of contrails. Contrails are thin, cirrus-like ice clouds that form when water vapor from aircraft engine exhausts mixes with extremely cold ambient air at high altitudes and rapidly condenses around particulate matter like soot, forming ice crystals. Contrails are responsible for approximately two-thirds of the net radiative forcing currently produced by the aviation industry (1). Radiative forcing is the difference between the amount of energy entering Earth's atmosphere from the sun and amount of energy leaving the atmosphere. An energy imbalance is created when heat gets trapped in the earth's atmosphere. Although contrails can produce a cooling effect during the daytime by reflecting incoming shortwave radiation, they exert a net warming effect by absorbing and re-emitting outgoing longwave radiation, particularly at night, creating an energy imbalance and contributing to global warming (2). As a result, contrails represent a major non-CO_2 climate impact of aviation. Figure 1 explains the various factors impacting the formation of persistent contrail cirrus clouds in the upper troposphere region of the atmosphere.

Contrail mitigation research tends to focus on flight path and altitude optimization as potential pathways, yet targeted deployment of SAFs is often seen as a supplementary solution in the field (4, 5). However, SAFs have the potential to significantly lower CO_2 emissions in the aviation industry. SAFs are renewable jet fuels that can be blended with conventional jet fuel without requiring new aircraft or fueling infrastructure. Increased adoption of SAFs could help the aviation industry progress toward its goal of net-zero emissions by 2050; for example, a sustained annual SAF growth rate of 1–2% could reduce aviation CO_2 emissions by 5.5–9.5% over 15 years (6). The effect of SAFs on contrail formation is complex and this research aims to address both positive and negative impacts of SAFs that can contribute to persistent contrails in the atmosphere.

Contrail formation begins when activated soot particles first form liquid water droplets through condensation. At temperatures near 235 K, the droplets freeze via homogeneous ice nucleation, forming ice crystals (7). Through these processes, both soot particle and water vapor emissions affect contrail formation frequency and contrail radiative forcing. SAFs can reduce the non-volatile particulate matter (nvPM) emissions index by up to 70%, while fleetwide adoption of 100% SAF could lower annual mean contrail net radiative forcing by 44% (8, 9). On the other hand, SAFs have higher water vapor emissions and can therefore also increase the frequency of contrail formation (10). Contrail formation is governed by both engine emissions and atmospheric conditions and occurs only when the Schmidt-Appleman criterion (SAC) is satisfied. The SAC defines the threshold at which the mixing of hot, moist aircraft exhaust with cold, ambient air leads to saturation with respect to liquid water (11, 12). The SAC depends on many parameters that vary with different fuels, including combustion heat, emission indices, and engine thrust. Different values for these will result in different temperature thresholds for contrail formation. Differences among fuels arise primarily from variations in the hydrogen-to-carbon ratio, combustion efficiency, and water vapor production per unit energy released. For example, hydrogen combustion produces substantially more water vapor per unit heat released than conventional kerosene, resulting in higher likeliness for contrail formation (13). Conversely, kerosene exhibits higher particle mass and number emissions, which enhance ice crystal number concentrations once contrails form (14).

Whether this threshold is met depends on ambient temperature and pressure, atmospheric humidity, engine efficiency, and the amount of water vapor emitted during fuel combustion (15). If ambient temperatures are insufficiently low, contrails will not form (13). Consequently, atmospheric conditions are critical in determining contrail formation and their associated radiative forcing. Atmospheric humidity and ambient temperature and pressure vary at different points of the atmosphere and on different flight routes. Contrails form in regions with high humidity and low temperatures. When relative humidity with respect to ice exceeds 100%, the atmospheric zone is called an ice-supersaturated region. These regions are ideal for the formation of

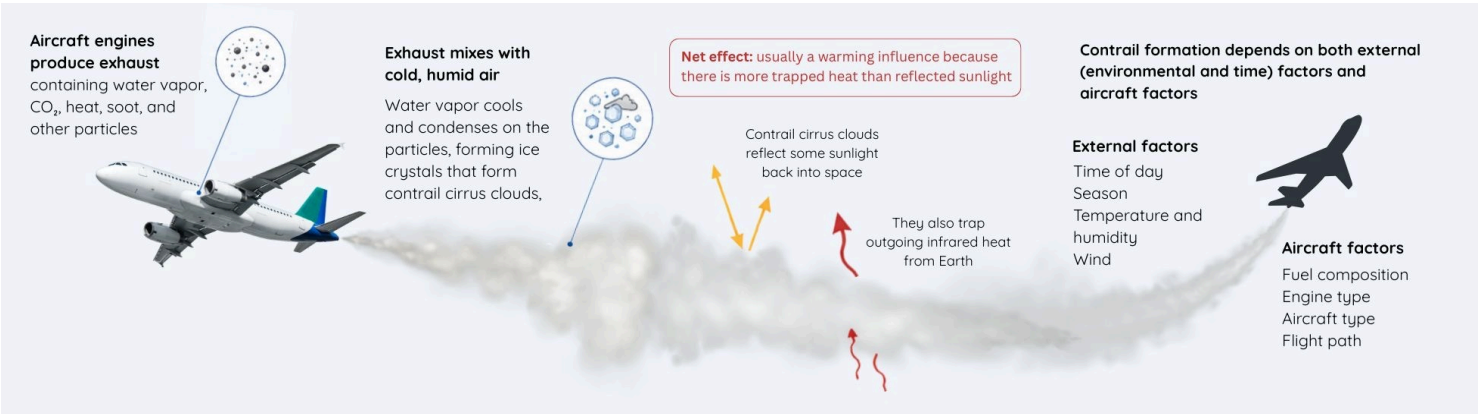

Figure 1. Contrail Cirrus Formation. Factors leading to contrail formation and positive radiative forcing.

cirrus clouds and the long-lasting persistence of contrails. It is important to examine the effects of SAFs on contrails, not at specific points, but on actual flight routes.

This paper aims to utilize the SAC to determine the effect of various SAF types on the temperature threshold for contrail formation, as well as apply this threshold on multiple routes to find the impact on actual contrail formation probability.

Methods

This research study combined a mathematical framework with a flight path modeling approach. The mathematical framework was utilized to have a rigorous handle on the threshold temperature calculation for different kinds of aviation fuels. These include kerosene (the baseline fuel), compared to Hydroprocessed Esters and Fatty Acids Synthetic Paraffinic Kerosene (HEFA-SPK), Fischer-Tropsch Synthetic Paraffinic Kerosene (FT-SPK), and Alcohol-to-Jet Synthetic Paraffinic Kerosene (ATJ-SPK), which are the most common types of SAFs currently being used. The flight modeling builds from the calculated threshold temperature and provides a way to understand relative impact of SAFs on flight routes of varying lengths.

Mathematical Framework

This framework was based on the SAC for contrail formation, as formulated by Schumann (13). Contrail formation is assumed to occur when the exhaust plume from an aircraft engine, mixing adiabatically with ambient air, becomes supersaturated with respect to ice. The threshold condition is defined by the critical ambient temperature, below which contrails form. The various factors that must be considered to determine threshold temperature include propulsion efficiency, slope parameter G, and the maximum temperature thresholds for liquid (T_{LM}) and ice-saturated formation (T_{IM}).

η is the propulsion efficiency of the aircraft which is dependent on engine type. It considers thrust (F), true air speed (V), specific combustion heat (Q), and rate of fuel flow (m_F).

$$\eta = \frac{FV}{Qm_F} \quad \text{(Eq. 1)}$$

The threshold temperature can be expressed in terms of slope parameter G, which characterizes the ratio of heat release to water vapor emission in the exhaust plume. This slope parameter is defined by:

$$G = \frac{EI_{H2O}c_p p}{\varepsilon Q(1-\eta)} \quad \text{(Eq. 2)}$$

ε is the ratio of gas constants or molar masses of dry air and water vapor and the value is taken as 0.622. c_p is the specific heat capacity and represents the exhaust gas temperature of modern jet engines. The value used in this study is 1050 J kg^{-1} K^{-1} at T = 600K., Other variables include the emission index of water vapor EI_{H2O} (the amount of water produced per unit fuel), the ambient air pressure at cruise altitude (p), and overall propulsion efficiency of the aircraft engine (η).

For the SAC, G is the thermodynamic parameter that describes how temperature decreases relative to water vapor increase when hot aircraft exhaust mixes with cold ambient air. Physically, it represents the slope of the exhaust-air mixing line in temperature-humidity space. This slope determines whether the mixture will reach saturation with respect to water during mixing. If the mixing line intersects with the saturation curve, condensation occurs, and a contrail can form. Thus, G directly controls the critical ambient temperature threshold for contrail formation.

A larger G means the mixture reaches saturation more easily, allowing contrails to form at relatively warmer temperatures. A smaller G requires colder ambient conditions for contrail formation. Therefore, G links aircraft engine thermodynamics with atmospheric conditions in determining when persistent contrails can develop.

Using G, T_{LM} and T_{IM} can be approximated using Equations 3 and 4. If the ambient temperature is higher than T_{LM}, no condensation occurs. If it is lower than T_{LM}, water droplets form, which generally freeze into ice crystals. If the temperature is lower than T_{IM} and the atmosphere is sufficiently humid, the contrail will persist and spread, which is the key factor in aircraft-induced radiative forcing and climate warming.

$$T_{LM} = -46.46 + 9.43\ln(G - 0.053) + 0.720[\ln(G - 0.053)]2 \quad \text{(Eq. 3)}$$

$$T_{IM} = -43.36 + 9.08\ln(G - 0.02) + 0.49[\ln(G - 0.02)]2 \quad \text{(Eq. 4)}$$

When relative humidity U = 1, $T_{(LM,\ IM)} = T_{(LC,\ IC)}$. When assuming relative humidity is at 100%, T_{LM} and T_{IM} can then be used as the threshold temperatures, where persistent contrails form at temperatures below T_{LM}. T_{LM}, T_{IM}, and G are used for calculating T_{LC} (liquid-condensation temperature).

$$T_{LC} = T_{LM} - x, x = -A + (A^2 + 2B)^{\frac{1}{2}}, \quad \text{(Eq. 5)}$$

$$with\ A = \frac{(1-U)G}{U^2 e_L^{'}(T_{LM})},\ B = \frac{e_L C - e_E}{U^2 e_L^{'}(T_{LM})},\ e_E = U_{e_L}(T_{LM})$$

e" is calculated from the Clausius-Clapeyron relationship, which estimates vapor pressure at different temperatures.
T_{LC} is the temperature at which the exhaust plume from an aircraft first becomes saturated with respect to liquid water as it mixes with the surrounding air. When the plume cools below T_{LC}, the water vapor emitted by the engine can condense into tiny liquid droplets.

For a visible contrail to form and persist, the ambient air temperature must be below T_{LC} so that condensation can begin. Contrails form when the surrounding atmosphere is cold enough that the mixing line of the exhaust plume crosses the ice saturation curve. Thus, T_{LC} marks the threshold for initial condensation, while

Table 1. Engine Parameters. CFM56-7B26 engine input parameters used to calculate propulsion efficiency, η.

	Unit	Value
Thrust per engine (*F*)	kN	32.295
True air speed (*V*)	m s^{-1}	233.89
Rate of fuel flow (*mF*)	kg s^{-1}	0.575
Relative humidity (*U*)	%	0.42

Table 2. Fuel Parameters. Combustion properties and values of kerosene and SAFs used in the analysis.

	Specific Combustion Heat (*Q*)	EI_{h2o}
kerosene (Baseline)	43.2	1.25
HEFA-SPK	44.1	1.37
FT-SPK	43.9	1.37
ATJ-SPK	44	1.38

T_{IC} determines whether those droplets freeze and create the ice crystals that make contrails visible and long-lasting. The T_{IC} can be calculated using the same formula as T_{LC} by replacing T_{LM} with T_{IM}. From this mathematical framework, key parameter values to be utilized during the flight modeling phase of the research were identified. The engine parameter values are based on one of the most commonly used commercial aircraft: a B737 equipped with a CFM56-7B26 engine (16,17).

Fuel parameters were calculated for kerosene, which is used as baseline fuel, and three commonly used sustainable aviation fuels. HEFA-SPK is produced by hydroprocessing biological feedstocks such as waste cooking oils, animal fats, or plant oils. It is currently the most commercially mature and widely available SAF and can be blended with conventional jet fuel at up to 50% without modification to existing engines. Experimental evidence from the Emission and Climate Impact of Alternative Fuels (ECLIF3) campaign has confirmed that 100% HEFA-SPK combustion reduces contrail ice crystal numbers by 56% compared to conventional Jet-A1 fuel, with modeled reductions in contrail radiative forcing of 26% (18). FT-SPK is produced via the Fischer-Tropsch process. The resulting fuel is highly refined with very low sulfur and aromatic content, contributing to notably reduced nvPM emissions relative to conventional kerosene. ATJ-SPK, produced by converting fermentation-derived alcohols, offers a flexible feedstock pathway, however, it currently has higher production costs than HEFA (19, 20).

Engine and Fuel parameters presented in Table 1 and Table 2 are consistent throughout all the routes modeled during this research. Table 3 presents an example calculation based on a flight at a pressure of 216.63 hPa. This calculation will change at different points in the flight based on flight altitude and atmospheric conditions.

Flight Modeling

The threshold temperature formula from the previous section was applied to specific routes to observe potential impact on contrail formation in an applied setting. Four representative routes were chosen to understand mitigatory effects of SAFs under varying atmospheric and fuel usage conditions. These include a long-haul, high latitude route (London–New York); a very long-haul, mid-to-high latitude route (Los Angeles–Tokyo); a medium-haul, subtropical latitude route (Paris–Dubai); and a short-haul, mid-latitude route (Berlin–Rome).

Flight paths for the four selected routes were constructed using the great circle method, which defines the shortest geodesic distance between two points on the surface of a sphere and serves as the standard geometric basis for long-haul aviation route planning. Since a great circle route requires continuous heading adjustment as it traverses the curvature of the Earth, direct implementation in flight simulations is not computationally feasible. Therefore, each route was discretized into a series of intermediate waypoints at regular intervals along the great circle arc, with each segment between consecutive waypoints approximated as a rhumb line of constant bearing (21). This waypoint-based discretization approach is well established in the aviation literature as a method for accurately representing geodesic flight trajectories and it helps maintain computational efficiency (22). The geographic coordinates of each waypoint, defined by latitude and longitude, were derived trigonometrically from the origin-destination airport pair using the haversine formula. This accounts for the spherical geometry of the Earth and has been validated for route distance calculations in global aviation fuel and emissions modelling (22). For each of the four routes, origin and destination coordinates were used from OurAirports database as shown in Table 4.

Atmospheric data (pressure, temperature, and relative humidity) for each waypoint was implemented through accessing the ERA5 atmospheric reanalysis data which is the fifth generation of climate data produced by the European Center for Medium range weather forecasts.

Table 3. Example calculations for contrail formation parameters for a flight at pressure of 216.63 hPa. Overall efficiency (η), thermodynamic factor (G), and critical threshold temperatures for kerosene and SAF alternatives at cruise pressure.

	η	G (Pa.K^{-1})	T_{LM} (°C)	T_{IM} (°C)	T_{LC} (°C)	T_{IC} (°C)
kerosene (Baseline)	0.3040852476	1.452438883	-43.21	-40.03	-43.95	-40.70
HEFA-SPK	0.2978794262	1.545602895	-42.57	-39.44	-43.27	-40.08
FT-SPK	0.2992365079	1.555651179	-42.50	-39.37	-43.19	-40.01
ATJ-SPK	0.2985564249	1.561929085	-42.46	-39.34	-43.15	-39.97

Table 4. Origin and destination Latitude and Longitude of 8 airports on 4 flight routes from Our Airports database (23). Latitude and Longitude for origin and destination airport used to calculate waypoints along the route.

IATA Code	Airport Name	Latitude	Longitude
LHR	London Heathrow	51.47001	-0.4543
JFK	New York JFK	40.6413	-73.7781
LAX	Los Angeles	33.9416	-118.4085
NRT	Tokyo Narita	35.7720	140.3929
CDG	Paris CDG	49.0097	2.5479
DXB	Dubai	25.2532	55.3657
BER	Berlin Brandenburg	52.3667	13.5033
FCO	Rome Fiumicino	41.8003	12.2389

This data was accessed by using the Copernicus Climate Data Store Application programming interface or API. Data averaged over three months (December, January, February) was used, as there is a higher likelihood of contrail formation during winter. The data was finally converted into a probability function that compares probability of contrail formation ($T_{IC} < T_{ambient} \leq T_{LC}$) and the impact of SAF type on each flight route. The probability was calculated from 0 to 1 based on threshold temperature and relative humidity across all waypoints on the flight route.

Results and Discussion

As a first step, the overall probability of contrail formation along each flight path was calculated. As contrail formation is governed by atmospheric temperature and humidity, which change with latitude and altitude, the four routes in different latitudinal bands could capture different atmospheric conditions (1).

Figure 2 presents the distribution of contrail formation probability along each of the four representative flight routes using baseline kerosene fuel. The color scale represents the likelihood of contrail formation at the waypoints along each flight route.

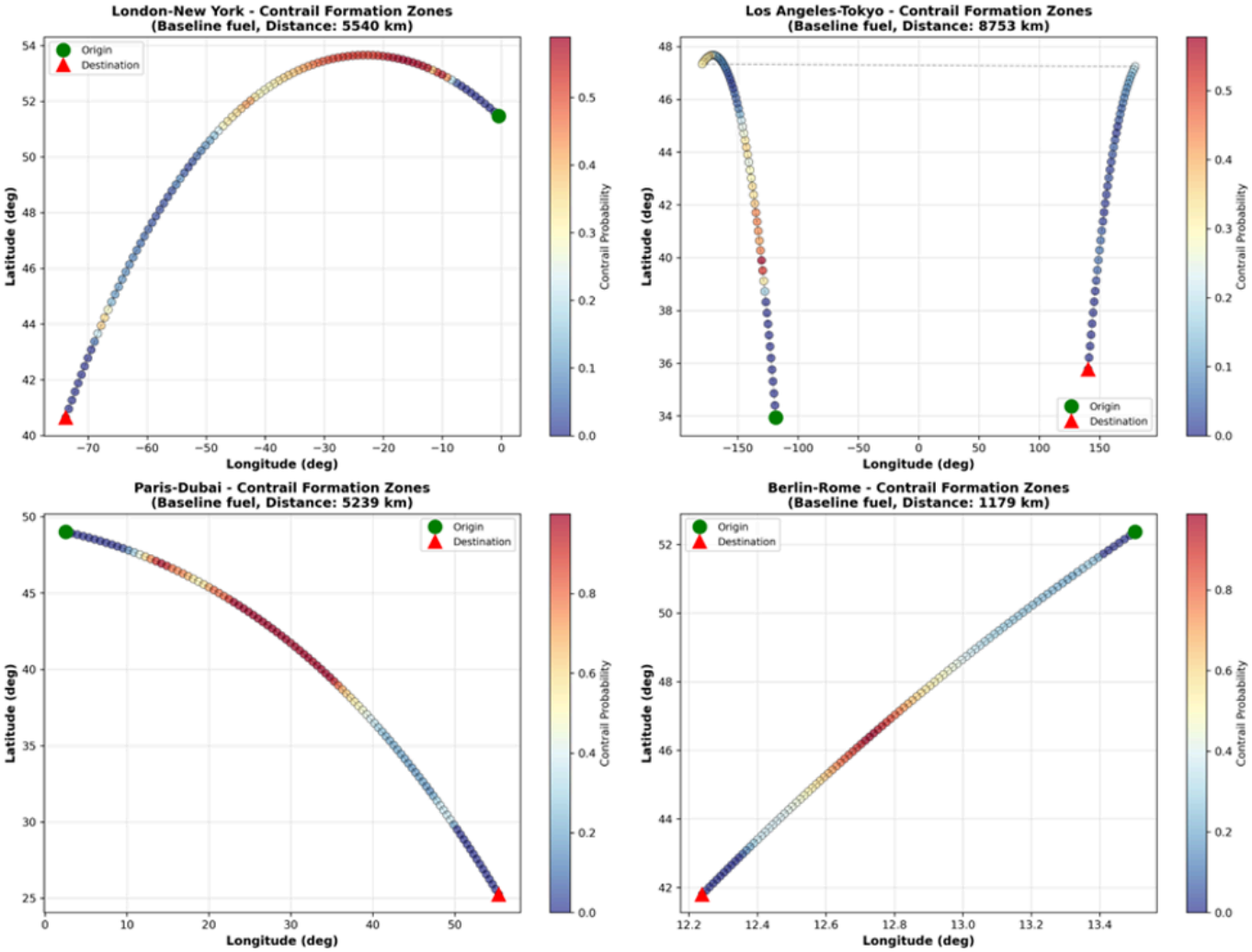

Figure 2. Probability of Contrail formation along the flight path on each route. Probability of 0.0 to 1.0 indicated at each waypoint along the flight path.

The London–New York route (5,540 km) exhibited a characteristic arc of elevated contrail probability concentrated along the high-latitude mid-route section, reaching peak values of approximately 0.5–0.6 near 54°N. This reflects the lower ambient temperatures encountered at high latitudes during transatlantic cruise, which more frequently satisfy the SAC threshold temperature condition. Probability falls toward zero near both endpoints as the route descends to lower latitudes where ambient temperatures are warmer relative to the threshold.

The Los Angeles–Tokyo route (8,753 km) demonstrated that the contrail formation probability is highest in the polar arc section of the route, concentrated in the first half of the flight where the great circle trajectory reaches its highest latitudes. This part of the flight path represents the extremely cold temperature where the SAC threshold is almost always met. As the route curved southward, probability decreased, reflecting the transition to warmer, drier subtropical conditions in the western Pacific. This asymmetry has implications for contrail avoidance strategies, as mitigation efforts on this route would be most effective during the departure phase.

The Paris–Dubai route (5,239 km) displayed the most pronounced latitudinal gradient, with high contrail formation probabilities near the origin at approximately 47°N, declining continuously toward the destination. Peak probabilities approached 1.0 in the northern section of the route over central Europe, where cold upper-tropospheric conditions and higher relative humidity consistently satisfy the SAC. This contrasts with near-zero probabilities closer to the Arabian Peninsula, where the warm and dry subtropical atmosphere provides strongly unfavorable conditions for contrail formation. This route therefore illustrates the strongest dependence on latitude of all routes studied.

The Berlin–Rome route (1,179 km) showed low contrail formation probability along most of its length. The short cruise phase limited exposure to cold upper-tropospheric air, and the mid-latitude trajectory over central Europe did not reach the high-altitude, cold conditions required to consistently satisfy the SAC. Even though peak contrail formation probability was high, it was a smaller proportion of the total route length when compared to contrail-forming conditions for the long-haul routes.

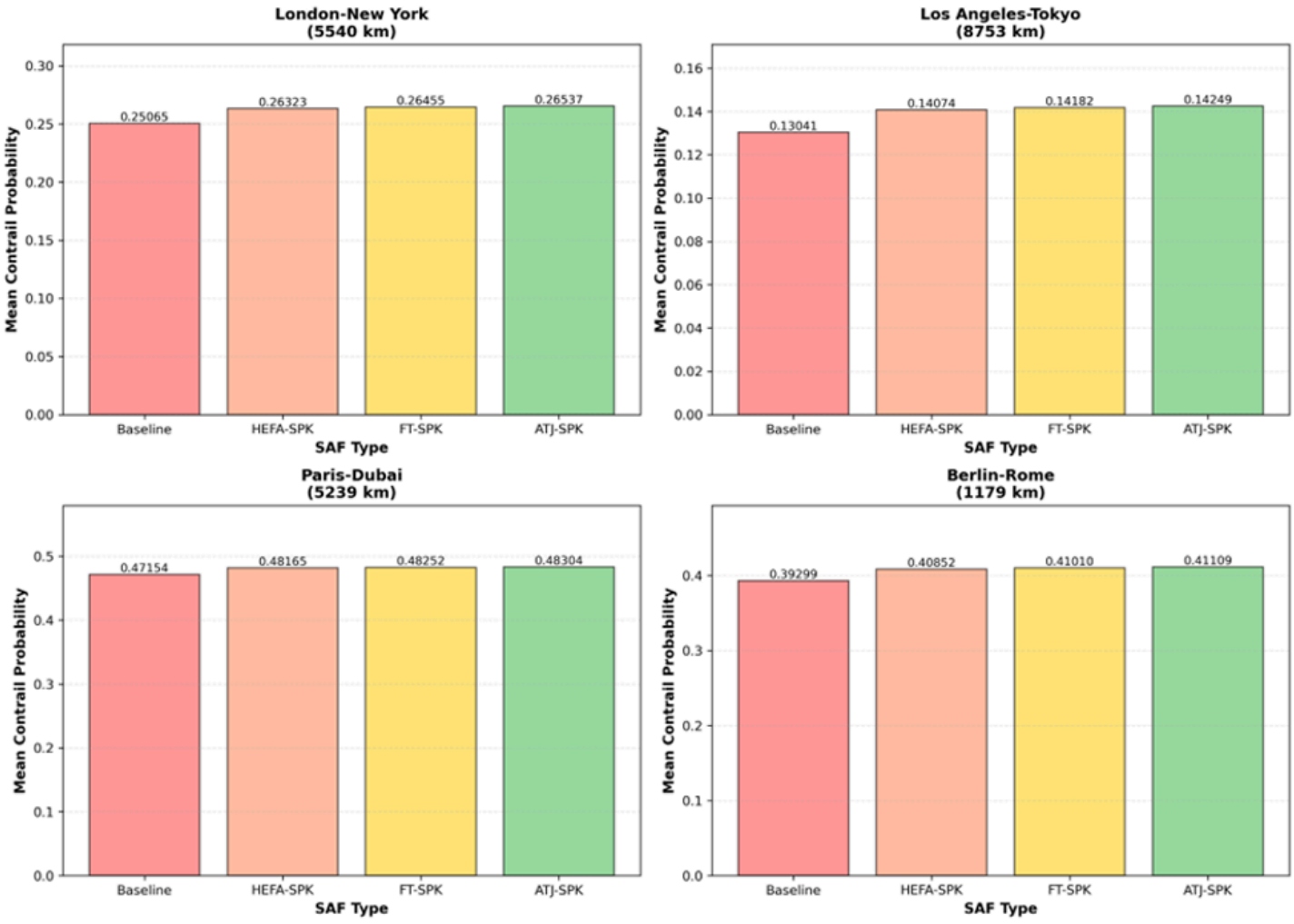

Figure 3. Mean Contrail Probability for kerosene and SAFs on flight routes. Mean Contrail Probability along each of the flight paths used to compare overall impact of SAFs, instead of along each waypoint on the routes.

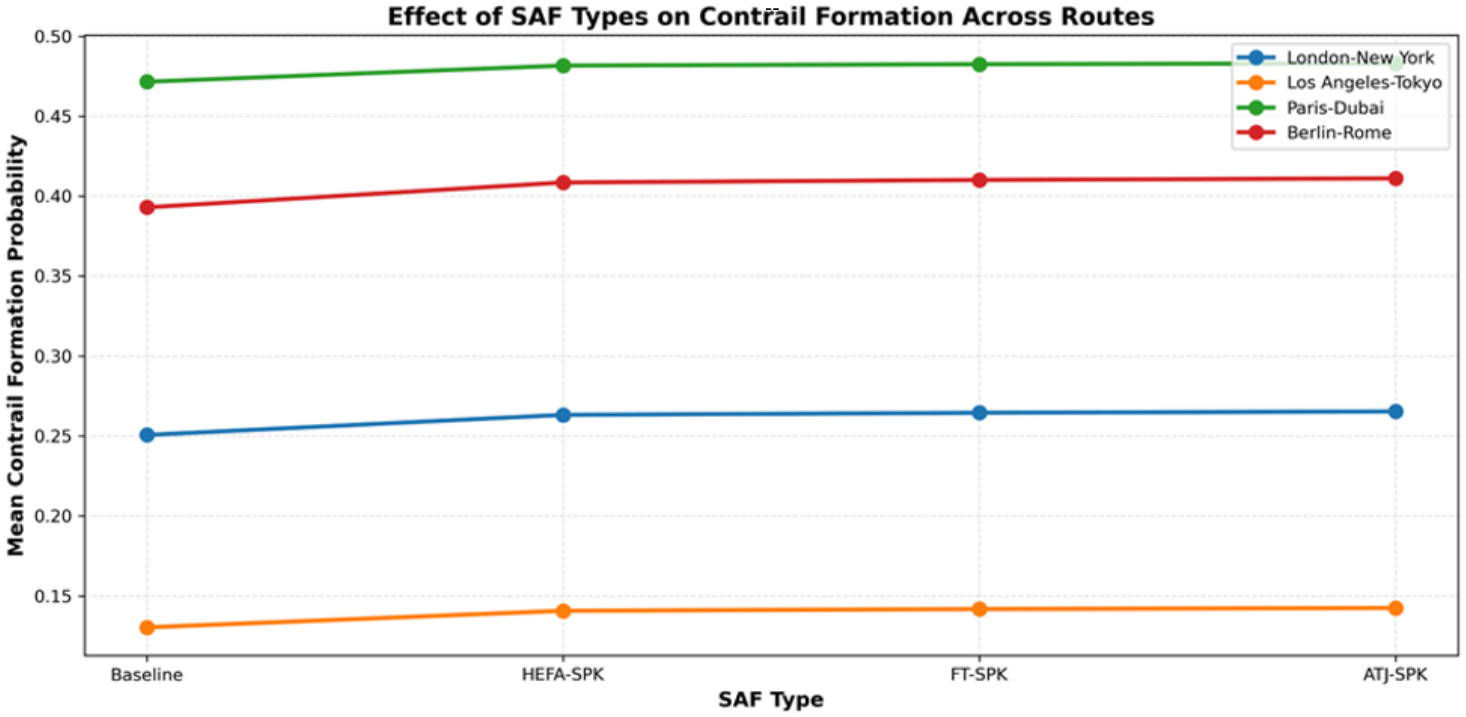

Figure 4. Effect of SAFs on mean contrail formation probability. Fuel types have similar impact on contrail formation across flight routes.

Taken together, the four routes supported that contrail formation probability is governed by ambient temperature, which, in turn, is driven by latitude and cruise altitude.

When studying the impact of SAFs on each of the routes, mean contrail probability for each route was utilized as an evaluative measurement. Figure 3 presents the mean contrail formation probability for each SAF type across the four representative flight routes, shown as bar charts per route. Figure 4 presents a combined line plot for cross-route comparison. Across all routes, mean contrail formation probability increased marginally from baseline kerosene to each SAF blend, with ATJ-SPK consistently recording the highest values, and HEFA-SPK the lowest among the three alternative fuels.

In Figure 3, for the London–New York route, mean probability rose from 0.251 for baseline kerosene to 0.265 for ATJ-SPK, representing an increase of 1.4 percentage points. A comparable pattern was observed on the Los Angeles–Tokyo route, where probabilities increased from 0.130 to 0.142 across the same fuel range. The Paris–Dubai route recorded the highest absolute probabilities of all four routes, rising from 0.472 for baseline to 0.483 for ATJ-SPK, consistent with the high-probability in the northern section of the route identified in Figure 1. The Berlin–Rome route similarly showed an increase from 0.393 to 0.411, which, while numerically larger than the London–New York shift, must be interpreted in the context of the short route length and limited total contrail exposure discussed previously.

This counterintuitive increase in contrail formation probability with SAFs is attributable to the thermodynamic properties of the fuels rather than a failure of mitigation. As shown in Table 3, SAFs exhibit higher water vapor emission indices and higher specific combustion heat relative to baseline kerosene. These properties combine to increase the slope parameter G, which shifts the SAC threshold temperatures T_{LC} and T_{IC} to slightly warmer values. This expands the range of atmospheric conditions under which the criterion is satisfied. This thermodynamic effect is well established in literature and has been noted as a trade-off inherent to the fuel chemistry of low-aromatic, synthetically derived aviation fuels (13, 24).

It is important to note that this thermodynamic effect acts in isolation within the current model framework. The primary mitigatory mechanism of SAFs is the reduction of nvPM emissions, which limits the availability of ice nucleation sites in the exhaust plume. This operates through a separate physical pathway not captured by the SAC threshold comparison alone. The results presented here therefore represent a conservative upper bound of all contrail formation and does not separate the persistent contrail formation that SAFs tend to mitigate. The net climatic impact of SAF deployment is expected to be beneficial when nvPM suppression of ice crystal nucleation is accounted for. This is discussed further in the conclusion section.

Figure 4 consolidates the cross-route comparison, and it supports that the fuel-related trend is consistent in direction across all routes but differs in magnitude. Paris–Dubai maintained the

highest mean probability throughout, followed by Berlin–Rome, London–New York, and Los Angeles–Tokyo. The parallel trajectories of all four routes across the fuel axis indicate that the thermodynamic response to SAF blend properties is route-independent. The shift in G affects threshold temperatures uniformly regardless of the atmospheric conditions encountered along a given trajectory.

Conclusion

This study assessed the mitigatory effects of three sustainable aviation fuels, HEFA-SPK, FT-SPK, and ATJ-SPK, on contrail formation across four representative flight routes. Contrail formation probability at each waypoint was determined by evaluating whether ambient temperature satisfied the SAC threshold condition. The threshold temperatures T_{LC} and T_{IC} were computed from fuel-specific thermodynamic parameters including propulsion efficiency, slope parameter G, and ambient relative humidity. The four routes were selected to span a representative range of operational conditions encountered in global commercial aviation, from high-latitude, long-haul corridors to short-haul, intra-European services.

Across all four routes, the thermodynamic properties of SAFs, specifically their higher water vapor emission indices and specific combustion heat relative to baseline kerosene, resulted in a marginal increase in mean contrail formation probability. The scope of this research was kept narrow to focus on the thermodynamic effect which shifts the SAC threshold temperatures T_{LC} and T_{IC} to slightly warmer values, broadening the range of atmospheric conditions under which the criterion is satisfied. This thermodynamic effect is well established in the literature and does not contradict the mitigatory potential of SAFs. The results presented here should therefore be interpreted as reflecting the thermodynamic component of contrail formation in isolation, in the absence of nvPM effects.

Several directions for future research emerge directly from the findings and limitations of this work. The immediate extension is the integration of nvPM emission indices into the probability framework. Combining the temperature threshold computation with a nvPM activation model to produce a net contrail formation probability will account for both thermodynamic and particle-based effects. This will also give probability for more persistent contrails rather than all contrails including transient ones. Additionally, current jet engines operate in what is known as the soot-rich regime, where a high concentration of nvPM particles are available to act as ice nucleation sites. In this regime, reducing nvPM emissions directly reduces the number of ice crystals that form, which produces a clear mitigatory benefit. However, as SAF blend ratios increase and nvPM emissions fall substantially, engines may transition into the soot-poor regime (25). Here, the relationship between nvPM concentration and ice crystal formation breaks down, and smaller volatile particles in the exhaust plume begin to take over as the main nucleation sites. Under these conditions, further reductions in nvPM no longer guarantee fewer contrail ice crystals. Understanding where this transition occurs and key factors affecting it is essential for confidently predicting the climate benefit of high-blend SAF usage.

A second area in need of further investigation is the sensitivity of route-level contrail formation probability to atmospheric data resolution. ERA5 reanalysis data, while widely used and validated, operates at approximately 31 km horizontal resolution. This is wider than the spatial scale of many ice-supersaturated regions, which can have horizontal extents of only a few kilometers (26). This limitation likely causes the model to underestimate both the frequency and variability of persistent contrail conditions, particularly on routes traversing complex regions such as the North Atlantic storm track. Higher resolution atmospheric data would better capture the variability of ice-supersaturated regions and reduce uncertainty regarding when and where contrail formation conditions are met along each route.

Finally, translating the threshold temperature-based formation probability metric developed here into a direct measure of climate impact presents a valuable extension of this work. The current framework weighs all contrail-forming waypoints equally, irrespective of the time of day, surface albedo, or season. These factors can substantially change the net radiative forcing of any given contrail (1,3). Incorporating radiative forcing weighting into the waypoint probability calculation would convert the metric from a formation indicator into a climate impact index. This will enable route-specific and fuel-specific recommendations to be expressed in terms of warming potential rather than formation frequency alone. Combined with targeted SAF deployment strategies, such a framework could directly inform airline fuel allocation decisions that maximize climate benefit of SAF used.

Acknowledgements

The author thanks Dr. Nafiz Chowdhary from Oxford Thermofluids Institute, University of Oxford for his guidance during this research.

References

1. D.S. Lee, D. W. Fahey, A. Skowron, M. R. Allen, U. Burkhardt, Q. Chen, S. J. Doherty, S. Freeman, P. M. Forster, J. Fuglestvedt, A. Gettelman, R. R. De León, L. L. Lim, M. T. Lund, R. J. Millar, B. Owen, J. E. Penner, G. Pitari, M. J. Prather, R. Sausen, L. J. Wilcox. The contribution of global aviation to anthropogenic climate forcing for 2000 to 2018. Atmos Environ 244, e117834 (2020). 10.1016/j.atmosenv.2020.117834
2. R. Meerkötter, U. Schumann, D. R. Doelling, P. Minnis, T. Nakajima, Y. Tsushima. Radiative forcing by contrails. Ann. Geophys. 17, 1080–1094 (1999).
3. J. Cathcart, A. Chen, J. Majholm, A. Jardine Wall. “Aviation Contrails: What We Know—and What We Don’t—about This Warming Phenomenon” (RMI, 2024); https://rmi.org/aviation-contrails-what-we-know-and-what-we-dont-about-this-warming-phenomenon/

4. E. Roosenbrand, J. Sun, J. Hoekstra. Contrail minimization through altitude diversions: A feasibility study leveraging global data. Transp. Res. Interdiscip. Perspect. 22, e100953. 10.1016/j.trip.2023.100953
5. J. Cathcart, A. Chen. “Contrail Mitigation: A Collaborative Approach in the Face of Uncertainty” (RMI, 2022); https://rmi.org/contrail-mitigation-a-collaborative-approach-in-the-face-of-uncertainty/
6. S. Sgouridis, P. A. Bonnefoy, R. J. Hansman. Air transportation in a carbon constrained world: Long-term dynamics of policies and strategies for mitigating the carbon footprint of commercial aviation. Transp. Res. A: Policy Pract. 45, 1077–1091 (2011).
7. B. Kärcher, U. Burkhardt, A. Bier, L. Bock, I. J. Ford. The microphysical pathway to contrail formation. J. Geophys. Res. Atmos. 120, 7893–7927 (2015).
8. L. Durdina, B. T. Brem, M. Elser, D. Schönenberger, F. Siegerist, J. G. Anet. Reduction of nonvolatile particulate matter emissions of a commercial turbofan engine at the ground level from the use of a sustainable aviation fuel blend. Environ. Sci. Technol. 55, 14576–14585 (2021).
9. R. Teoh, U. Schumann, A. Majumdar, M. E. J. Stettler, M. E. J. Targeted use of sustainable aviation fuel to maximize climate benefits. Environ. Sci. Technol. 56, 17246–17255 (20220.
10. M. Narciso, J. M. Melo de Sousa. Influence of sustainable aviation fuels on the formation of contrails and their properties. Energies, 14, e5557 (2021). 10.3390/en14175557
11. E. Schmidt. (1941). Die Entstehung von Eisnebel aus den Auspuffgasen von Flugmotoren [The formation of ice fog from the exhaust gases of aircraft engines]. Schriften der Deutschen Akademie der Luftfahrtforschung 44, 1–15 (1941).
12. H. Appleman. The formation of exhaust condensation trails by jet aircraft. Bull. Am. Metero. Soc. 34, 14–20 (1953).
13. U. Schumann. On conditions for contrail formation from aircraft exhausts. Meteorologische Zeitschrift 5, 4–23 (1996).
14. G. Quante, C. Voigt, M. Kaltschmitt. Targeted use of paraffinic kerosene: Potentials and implications. Atmos. Environ.: X 23, e100279 (2024). 10.1016/j.aeaoa.2024.100279
15. B. Kärcher, C. Voigt. Susceptibility of contrail ice crystal numbers to aircraft soot particle emissions. Geophys. Res. Lett. 44, 8037–8046 (2017).
16. R. Balas, C. Danilet, M. Stefan. “Boeing aircraft overview 2025: Complete fleet guide. The Flying Engineer (2025).” https://theflyingengineer.com/boeing-aircraft-overview/
17. “AM International CFM56 — engine specs & aircraft. PlaneFYI.” https://planefyi.com/engines/cfm56/
18. S. Märkl, C. Voigt, D. Sauer, R. K. Dischl, S. Kaufmann, T. Harlaß, V. Hahn, A. Roiger, C. Weiß-Rehm, U. Burkhardt, U. Schumann, A. Marsing, M. Scheibe, A. Dörnbrack, C. Renard, M. Gauthier, P. Swann, P. Madden, D. Luff, P. Le Clercq. Powering aircraft with 100% sustainable aviation fuel reduces ice crystals in contrails. Atmos. Chem. and Phys. 24, 3813–3837 (2024).
19. E. Cabrera, J. M. Melo de Sousa. Use of Sustainable Fuels in Aviation—A Review. Energies 15, e2440 (2022). 10.3390/en15072440
20. ICAO Committee on Aviation Environmental Protection. “Assessment report on fuel composition effects on non-volatile particulate matter (nvPM) emissions” (International Civil Aviation Organization, 2022); https://www.icao.int/sites/default/files/sp-files/environmental-protection/Documents/ScientificUnderstanding/ICAO-CAEP12-Assessment-Report-on-fuel-composition-effects-on-nvPM-emissions.pdf
21. E. Williams (2024). Aviation Formulary V1.47
22. K. Seymour, M. Held, G. Georges, K. Boulouchos. Fuel estimation in air transportation: Modeling global fuel consumption for commercial aviation. Transp. Res. D: Transp. Environ.88, e102528 (2020). 10.1016/j.trd.2020.102528
23. Our Airports. "OurAirports Data" (OurAirports, 2024); https://ourairports.com/data/
24. J. Ponsonby, L. King, B. J. Murray, M. E. J. Stettler. Jet aircraft lubrication oil droplets as contrail ice-forming particles. Atmos. Chem. and Phys. 24, 2045–2058 (2024).
25. B. Kärcher, F. Yu. Role of aircraft soot emissions in contrail formation. Geophys. Res. Lett. 36, e01804 (2009). 10.1029/2008GL036649
26. K. Gierens, P. Spichtinger. "On the size distribution of ice-supersaturated regions in the upper troposphere and lowermost stratosphere." Ann. Geophys. 18, 499–504 (2000).